Master of Science

Development of an *in vitro* cell sheet-based anti-cancer model

세포시트 기반 생체외 암 모델의 개발

The Graduate School

of the University of Ulsan

Department of Medicine

Jaewang Lee

Development of an *in vitro* cell sheet-based anti-cancer model

Supervisor: Prof. Jong-Lyel Roh

A Dissertation

Submitted to

the Graduate School of the University of Ulsan

In partial Fulfillment of the Requirements

for the Degree of

Master of Science

By

Jaewang Lee

Department of Medicine

Seoul, Korea

December, 2018

Development of an *in vitro* cell sheet-based anti-cancer model

This certifies that the dissertation

of Jaewang Lee is approved.

Yoo Myungsang

Commitee Chair Dr.

Roh Jonglyel

Committe member Dr.

Kwon Minsu

Committee member Dr.

Department of Medicine

Seoul, Korea

December, 2018

ABSTRACT

Development of an *in vitro* cell sheet-based anti-cancer model

Jaewang Lee
Department of Medicine
The Graduate School of the Ulsan University

Cancer is one of the main causes of death in humans. Research on cancer has been done a lot since the 20th century until the 21st century, but has yet to fully understand it. While the two-dimensional model developed in these situations is used as a standard model for many cancer studies, these two-dimensional models do not reflect the actual cancer environment. Because of these shortcomings, 3D models, similar to the actual environment, are being developed to be applied to patients based on results from the two-dimensional model. However, these three-dimensional models were also totally not considered in the real world of the ECM, which exists in the body, only by using cancer cells to study the form of spheroid, or by mixing different cells. Only recently are these models being developed, and we also developed a cellular sheet-based three-dimensional model with our own technology of cell sheets. The cell sheet is an artificial tissue that mimics the tissue in the body and has been developed to help recover the unrelenting wounds of postoperative patients, burns and diabetes. The research was conducted in the belief that cell sheets could be combined with speroid to create an artificial environment similar to the actual cancer environment. In our study, unlike in the two-dimensional or simple spheroid culture, the presence of the ECM on cell sheets has shown to increase resistance to anticancer drugs in the cancer. Also, in the cellular sheet binding model of transversed insurer cells, the cell sheet model could be seen spreading around the invoice, unlike the former models. In addition, it was possible to observe the hypoxia area inside one of the main characteristics of cancer in the existing three-dimensional models. The EMT-related representative molecules like vimentin, TGF-β1, N-cadherin were analyzed through RT-qPCR and Western blot, and the results were shown that three molecules increased. Furthermore, stability could not be established in a traditional two-dimensional model. However, stability of a three-dimensional model created using cancer tissue from patients could be maintained up to 30 days. In addition, through the transduction of GFP into tissue, live area can

be confirmed with fluorescence in real time. This allowed us to identify the impact on cancer tissues over time in a five-day anti-cancer reaction. This is expected to help select an anti-cancer drug for each of patient.

keyword : Head and neck cancer, drug testing, cell sheet, *in vitro* 3D model, Invasion

Table of Contents

List of Figures

Introduction

1.1 2D *in vitro* cancer model and 3D *in vitro* cancer model

Two-dimensional (2D) *in vitro* cancer model is conventionally used to test and screen effectiveness of drugs. It is possible for a researcher to confirm the response of cancer from a specific drug fast. Also, many analytic methods have been developed for 2D cancer models. However, there is one big problem that is recapitulating the natural tumor microenvironment. This limitation have led the development of three-dimensional in vitro cancer model like spheroid.

Three-dimensional (3D) in vitro cancer model is more similar to the feature of cancer tissue than 2D in vitro cancer model. For example, 3D cancer models have the characteristic of real cancer tissue, such as hypoxia region, drug resistance, and the aggressive cells of outer surface. Actually, 2D in vitro cancer model is more sensitively respond than 3D model, but the real tissue is less sensitive than 2D. This is because while the former is directly affected all surface, the latter is only partially exposed because of aggregating morphology [1]. These characteristics reflect some of the characteristics of the actual cancer tissue. Moreover, 3D model has the advantages that it can reproduce the natural tumor composition and microenvironment by mixing with other cells. But 3D model also has limitations that it does not reflect all the peculiarity of actual tissues.

1.2 Cell sheet and scaffold

Cell sheets are known as tissue mimic, and used to cover and heal the defect from surgical wound. They consist of epithelial layer and sub-epithelial layer that includes fibroblasts and/or endothelial cells. Morphology is almost the same of tissue, except immune cells, muscle tissue, and adipose tissue. Especially, sub-epithelial layer is commonly mentioned as scaffold which is a supporting body of cells. Present, many scaffold exist, such as hydrogel, collagen gel, fibrin gel, and gelatin gel [2].

Scaffolds have attaching molecule that helps cells to be stable and change active form. They also affect wound healing or cancer survival, so are dealt with as a key factor. On top of that, they have the spaces that can accommodate a various of cells. For this reason, these day other cell as co-worker add to scaffolds to make the in vitro model like more real.

1.3 Tumor microenvironment

Tumor is surrounded by microenvironment, and interacts with neighbouring nonmalignant cells of the tumor stroma. Cells around microenvironment include fibroblasts, endothelial cells, and pericytes, all of which are embedded in a unique extracellular matrix. Tumor stroma consisting of microenvironment helps cancer survival and makes cancer have the resistance of anti-cancer drugs [1,3]. Especially, cancer-associated fibroblasts (CAFs) and tumor-associated macrophages (TAMs) are known as a key helper of tumor survival. Since tumor microenvironment have the diversity and complexity of component, a lot of research is bening done. Its regulation will be important for treatment and provide understanding more depth cancer biology.

1.4 Cancer-associated fibroblasts (CAFs)

CAFs are known as a important contributor in producing a reactive stroma that frequently maintain a tumour-promoting, tissue-repair response in solid tumors. CAFs mainly derive from tissue-resident fibroblasts that, under the influence of transforming growth factorβ (TGFβ), acquire the attribute of functional hyperactivation, including enhanced proliferation and motility, along with robust ECM biosynthesis and a deposition ability of collagens. Indeed, CAFs secrete enzymes, such as lysyl oxidases (LOXs) and hydroxylases, which catalyse the cross-linking of collagens to elastin and other ECM molecules. By controlling the bio-mechanical properties of the tumor stroma, including stiffness, elasticity and interstitial fluid pressure, CAFs indirectly modulate vascularization and blood flow in tumors. CAFs have well-established pro-angiogenic functions in tumours. They often colocalize with TABVs in human cancers, and co-implantation of CAFs and cancer cells enhances angiogenesis, decreases cancer cell dormancy and accelerates tumour growth in mice. CAFs are a major source of tumour VEGFA, but can also support tumour angiogenesis in a VEGFA-independent manner. CAF-derived PDGFC sustains angiogenesis by further stimulating CAFs to secrete pro-angiogenic growth factors, such as FGF2 and osteopontin. The CAF secretome potentiates tumour angiogenesis also by attracting vascular ECs and recruiting monocytes from the bone marrow, for example, through the CXCL12–CXCR4 axis. In melanoma, aged CAFs secrete the WNT antagonist secreted frizzled-related protein 2 (SFRP2), which exacerbates the angiogenic and malignant behaviour of tumours in old individuals124. Although CAFs also secrete

angiogenesis inhibitors, such as THBS1, tumours may overcome their angiostatic properties by adaptively increasing the production of pro-angiogenic factors [3,4].

1.5 Epithelial-mesenchymal transition (EMT)

Epithelial–mesenchymal transition (EMT) is an important event during development process by which epithelial cells acquire mesenchymal, fibroblast-like properties and show reduced intercellular attachment and enhanced motility. Through this process, each part of the body is placed appropriately. However, this incident can produce completely different results in the case of the development of cancer. Growing evidence shows a key role of EMT-like events during tumor progression and the transition of a tumor property from benign to malignant, which gives the initiating cancer cell with invasive and metastatic properties. Thus, it makes cancer therapy difficulty and causes the reduced survival rate of patients. EMT-related factors are known, such as vimentin, E-cadherin, N-cadherin, and TGF-β1. The expression level of TGF-beta1, vimentin, and N-cadherin rise during EMT process, but E-cadherin decline. These changes of molecules induce EMT. EMT-related signal pathway commonly comes to light, such as Wnt/β-catenin, Notch, TGF/smad, Ras, and PI3K/AKT. Especially, activation of the phosphatidylinositol 30 kinase (PI3K)/AKT axis is emerging as a central feature of EMT [5].

1.6 Tumor explant model

Tumor explant model has been developed to resolve the limitation of two-dimensional (2D) model or three-dimensional (3D) model. Tumor explant has tumor microenvironment affecting tumor survival in itself. So, tumor explant model can apply to the development of personalized medicine and assessing mono- or combinatorial treatments. The representative example of tumor explant model is patient-derived xenograft (PDX) mouse models. PDX improves a predictive accuracy of drugs. However, PDX also has problems that it needs a number of mice and a high cost. Above all, all primary human patient-derived tumors cannot be generated to PDX and the researchers have to select tumors through continuous maintenance that adapt to grow in an immunodeficient mouse. What this suggests that it takes for a long time to obtain established tumors, thus cost-effectiveness is very low in pre-clinical studies.

1.7 Hypoxia

Hypoxia is a state of low oxygen. Tumor mass has hypoxia region in a center of it. This is one of the main feature of tumor and occur by a deficient of nutrient and oxygen. Hypoxia makes cells excrete HIF-1α and TGF-β1 from neighbor cells like fibroblasts. These molecules stimulate cancer cells make neovascularization or move to other sites, so, called EMT process. Also, Hypoxia is known as chemoresistance related factor. The more hypoxic condition increase, the more chemoresistance rise. Thus hypoxia is very important factor.

1.8 A summary of this thesis

The aim of this thesis is to develop the three-dimensional (3D) in vitro model for cancer treatment or studies by using cell sheet which is tissue mimic. To summarize the whole thesis, combination the cancer spheroid or cancer tissue with the cell sheet can makes almost a similar character of the real tissue, but impossible in two-dimensional (2D) model. This feature makes that it will be possible for people to expect a effective of specific drug. Particularly, unlike a simple 3D model and 2D model, cell sheet based 3D model have sub-epithelial layer mentioned as scaffolds or extracellular matrix (ECM) related to survival or activation and have more chemoresistance like a real tissue. In addition, by using it we can maintain and be possible to observe the survival of cancer for a long time. Also, we can visualize hypoxia, viable cell, and epithelial-mesenchymal transition (EMT) using immunofluorescence. The results showed that the cell sheet based 3D *in vitro* model kept the features of cancer, gave cancer a chemoresistance in the death concentration of 2D model, and increased the expression level of genes which are associated with EMT. Finally, we examined the stability and viability in the real tissue 3D model.

2. Materials and Methods

2.1. Cell lines, reagents, and tissue

Three head-and-neck cancer (HNC) cell lines-ANC-HN3, HN4, and HN9-which were established in our hospital, were used in this study. The cell lines were authenticated using short tandem repeat-based DNA fingerprinting and multiplex polymerase chain reaction (PCR). The cells were cultured in Eagle's minimum essential medium or Roswell Park Memorial Institute 1640 (Thermo Fisher Scirentific, Waltham, MA, USA) with 10% fetal bovine serum at 37 ℃ in a humidified atmosphere containing 5% CO_2. the cells were then exposed to cisplatin (Sigma-Aldrich, St. Louis, MO, USA) or sorafenib (Santa Cruz, Biotechnology, Dallas, TX, USA) for the indicated time and at the indicated dose.

2.2. Gerneration of cancer spheroid and 3D mucosal sheet model

Cancer spheroids were generated using centrifugation to aggregate tumor cells under the non-adherent condition of the culture plate. A single-cell suspension of 5 x 10^3 cells/well was loaded into each well of ultralow-attachment, round-bottom culture plates (Corning Inc., Corning, NY, USA). Cell aggregation to obtain aggregates ~200 μm in diameter was facilitated by centrifugation of the plate at 1,000xg for 10 min. Tumor cells mixed with CAFs (1:3) were also used to generate spheroids, using the same method.

The 3D cancer cell-sheet model was generated by incorporating a cancer spheroid into an oral mucosal cell sheet using the described in our previous reports. This study was approved by the institutional reviwe board, and written informed consent was obtained from all participants. Briefly, small oral mucosal samples were harvested from patients who underwent trans-oral surgery. Blood (10 mL) from these patients was collected into vacutainer tubes (BD Bioscience, Franklin Lakes, NJ, USA) and the plasma was obtained by centrifugation. After washing, sterilizing, and dissociating the mucosa samples using enzymes and mincing cancer tissue using NO.15 blade, the epithelial layers were separated, and the oral keratinocytes and fibroblasts were cultured in vitro. For generating the 3D cancer cell-sheet model, a mixture of a plasma fibrin matrix and cultured fibroblasts was solidified in Transwell ® cell-sulture inserts with a 0.4-mm-pore polyester membrane (Corning) at 37 ℃ for 60 min. The inserts, medium, and supplements were placed in the plates. Tumor

spheroids and tumor were overlaid on the fibrin matrix containing normal oral fibroblasts, and the cultured keratinocytes were seeded onto the fibrin matrix and tumor spheroid. The sheets were grown under air-liquid interface culture conditions. The tumor spheroids and 3D cell sheet were cultured for 3 days and then exposed to vehicle (control), 10 μM sorafenib, 20 μM cisplatin for 3 days., 20 μM cisplatin or 20 μM docetaxel for 5 days. Each experiment was conducted in triplicate.

2.3. Cell viability assays

Following exposure to cisplatin and sorafenib, cell viabilitywas asseseed using the cell counting kit-8 (CCK-8; Dojundo Molecular Technologies, Inc., Tokyo, Japan) according to the manufacturer's instructions. Control cells were exposed to an equivalent amount of vehicle. Cancer spheroids or cultured tumor cells were incubated in the CCK-8 solution for 4h, and the supernatants were transferred o 96-well plates. Cell viability was assessed by measuring the absorbance at 450 nm using a SpectraMax M2 microplate reader (Molecular Devices, Sunnyvale, CA, USA). In addition, cell viability was evaluated by using the LIVE/DEAD assay. First, tumor spheroids or tumor micro-dissected from the 3D cell sheet were washed twice with 1x Hank's balanced salt solution (HBSS; Sigma-Aldrich, St. Louis, MO, USA). Cancer spheroids or 3D cell sheets were incubated with 8 μg/mL calcein-AM (Corning) and propidium iodide (Sigma-Aldrich) in a dark room at 37 ℃ for 1 h. After washing twice with 1x HBSS, the spheroids and sheets were observed using a fluorescence microscope (Zeiss, Oberkochen, Germany) at an absorbance of 514 nm or 632 nm, respectively.

2.4. Visualiztion of hypoxia in the 3D cell-sheet model

Hypoxia cells in the 3D cancer-cell sheet were observed using the LOX-1 hypoxia probe (Organogenix Inc., Kanagawa, Japan). A 20-μM probe solution was added to the cell culture media at a final probe concentration of 2 μM. After incubation at 37 ℃ for 24 h, red phosphorescence in the 3D cell-sheet model was obeserved using a fluorescence microscope (Zeiss) at an absorbance of 616 nm. The cell sheet was also stained with 8 μg/mL calcein-AM (Corning) for co-visualization of viable cells. The area of live cells in the cancer-CAF , tissue, and treatment groups was compared with that of the control of the cancer alone and the hypoxic cell areas relative to the control of cancer only or cancer with CAF group.

2.5. Green fluorescent protein gene transfection

To observe the migration of cancer cells in the 3D cell sheet and select a certain tissue fragments, ANC-HN3 cells and tissue were transfected with a green fluorescent protein (GFP) vector, pGFP (Takara Korea Biomedical Inc., Seoul, Korea), by using Lipofectamine® 2000 reagent (Thermo Fisher Scientific, Carlsbad, CA, USA) according to the manufacturer's protocol. A spheroid was made from ANC-HN3 cells transfected with pGFP, with or without CAFs (1:3), and the mucosal cell-sheet model as described above. The growth and migration of tumor cells from the spheroid embedded in the cell sheet were observed using a fluorescence microscope (Zeiss) at an absorbance of 509 nm. Changes in viability, size, and growth area of the spheroid with or without CAFs grown in the 3D cell-sheet model were calculated. The cancer area included the spheroid plus the invasion region of the fibrin matrix. The size and area of the spheroid were compared with those on day 0.

2.6. Reverse transcription-quantitative polymerase chain reaction and immunoblotting

For mRNA and protein extraction, cancer spheroid and their expanding tumor areas in 3D cell-sheet models were micro-dissected under a microscope. Total RNA was extracted from cancer spheroids or from tumors that were micro-dissected from 3D cell sheets using a total RNA extraction kit (Thermo Fisher Scientific) according to the manufacturer's instructions. Reverse transcription quantitative polymerase chain reaction (RT-qPCR) from 1-2 μg total RNA for each extracted sample was conducted using a SensiFAST™ SYBR® No-ROX Kit (Bioline International, Toronto, Canada) after cDNA synthesis using the $2^{-\Delta\Delta ct}$ method and normalized against *ACTB* mRNA levels. For western blotting, cancer spheroids or tumor micro-dissected from 3D cell sheets were lysed in cell lysis buffer (Cell Signaling Technology, Danvers, MA, USA) at 4 ℃ with a protease/phosphatase inhibitor cocktail (Cell Signaling Technology). Five to 15 μg of protein was resolved by electrophoresis on 10%-15% gels, transferred to nitrocellulose or polyvinylidene difluoride membranes, and probed with primary and secondary antibodies. The following primary antibodies were used: anti-TGF-β1 (R&D System, Minneapolis, MN, USA), vimentin (Cell Signaling Technology), and anti-N-cadherin (BD Bioscience, San Jose, CA, USA). β-actin (BS6007M, BioWorld, Atlanta, GA, USA) served as the loading control. All antibodies were diluted to from 1:250 to 1:5000.

2.7. Statistical analysis

The data were presented as the mean±standard error or deviation. The statistical significance of the differences between treatment groups was assessed using the Mann –Whitney U-test in SPSS 24.0 (IBM Corporation, Armonk, NY, USA). Statistical significance was defined as a two-sided P value<0.05.

3. Results

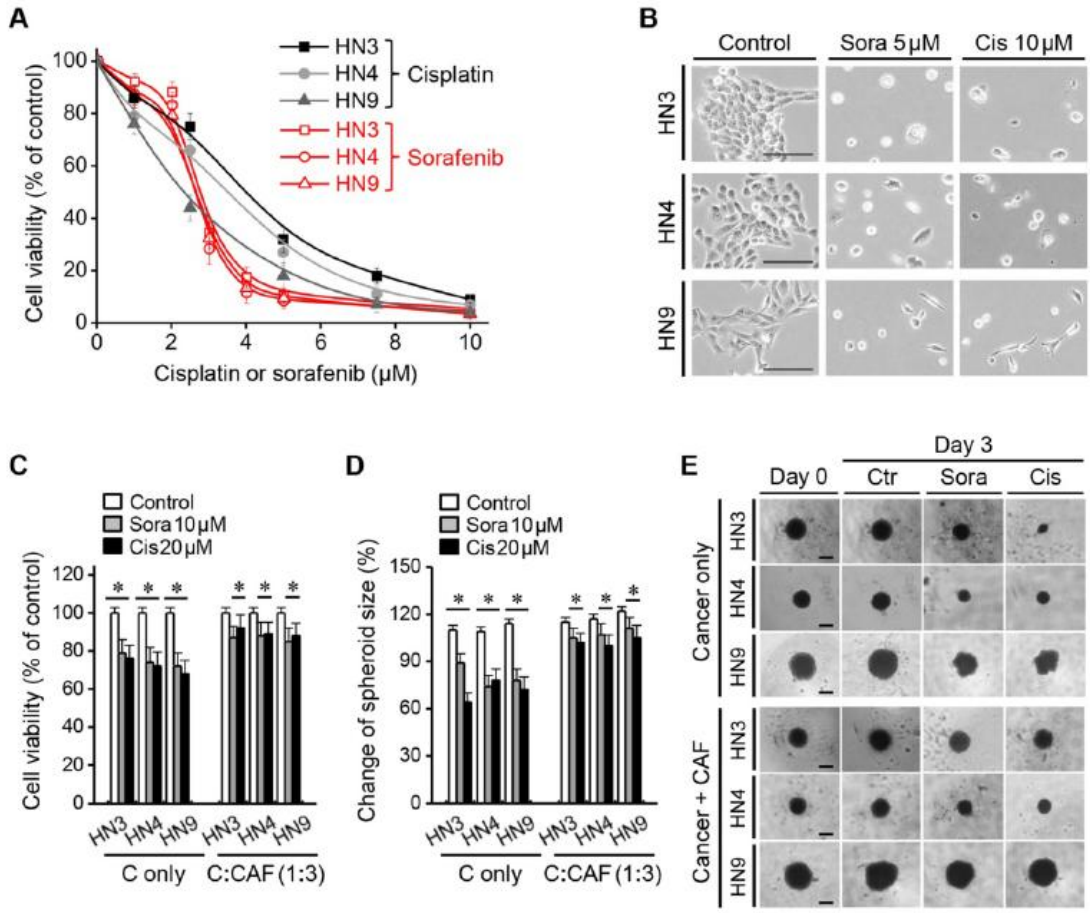

Fig. 1 Cancer-associated fibroblast (CAF) incorporation in a cancer spheroid causes resistance to chemotherapeutic agents. (A-B) Viability of head-and-neck cancer cells HN3, HN4, and HN9 in a two-dimensional culture dish exposed to different concentration of cisplatin (cis) or sorafenib (sora) for 72 h. Bars in cell images indicate 50 μm. (C-E) viability and size changes in cancer spheroids without (C only) or with CAFs (C:CAF = 1:3) exposed to 10 μM sorafenib or 20 μM cisplain for 72 h. Spheroid size on day 3 was compared wth that on day 0. The error bars represent the standard deviation from three replicates. * P<0.05 relative to the control or the drug treatment groups of C only. Bars in spheroid images indicate 100 μm.

3.1. Cancer spheroid and CAF incorporation promote resistance to chemotherapeutic agents

The half-maximal inhibitory concentrations (IC_{50}) of sorafenib and cisplatin were 2.5-2.7 μM and 2.2-4.7 μM, respectively, for the three HNC cell lines grown in 2D culture plates. More than 90% of HNC cells died following treatment with <5 μM sorafenib and 20 μM cisplatin) in subsequent experiments with cancer spheroids or 3D cell sheets. The viability of cancer spheroids after sorafenib or cisplatin treatment was much higher than that of HNC cells grown in 2D culture (**Figure 1C**). Incorporation of CAFs into the cancer spheroid (tumor:CAF = 1:3) resulted in even stronger resistance to 10 μM sorafenib or 20 μM cisplatin. After treatment with sorafenib and cisplatin for 3 days, cells viabilities were 72%-79% and 68%-76% in HNC spheroids without CAFs, respectively, and 85%-92% in HNC spheroids with CAFs, respectively (all $P<0.05$) (**Figure 1D-E**).

3.2. Cancer-CAF spheroid or cancer tissue in the 3D cell sheet shows enhanced invasive characteristics

A 3D cancer cell-sheet model was successfully generated by embedding cancer spheroids or cancer tissue into an oral mucosal cell sheet (**Figure 2A, Figure S1, and Figure 7B**). A cancer spheroid with pGFP-transfected HN3 cells was well visualized as green fluorescence. Cancer spheroids with CAFs appeared to be bigger and more invasive than those without CAFs (**Figure 2B**). Cancer spheroids with CAFs were more likely to spread into the fibrin matrix in the 3D cell-sheet model than those without CAFs (**Figure 2C**). Cell viability after treatment with sorafenib or cisplatin did not significantly differ between 3D cell sheets containing cancer spheroids with CAFs and those without CAF incorporation ($P<0.05$).

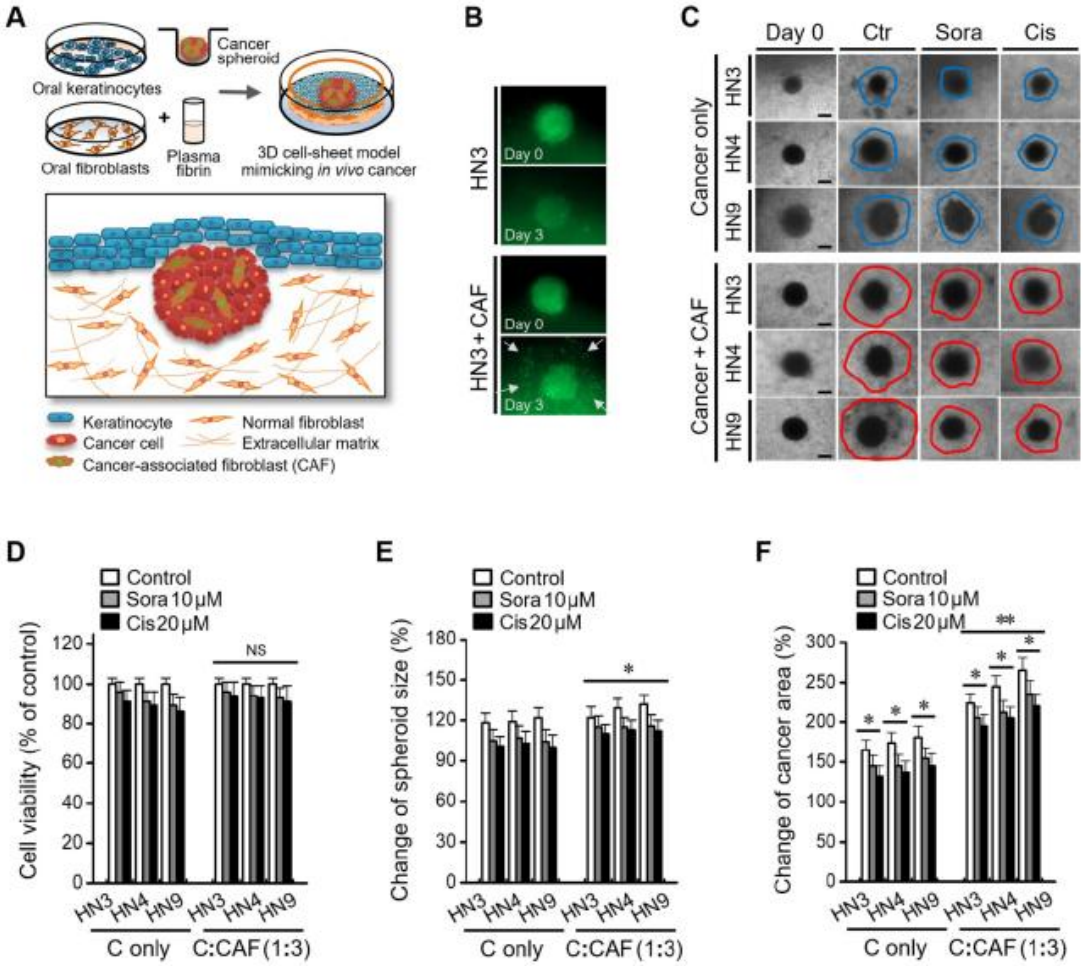

Fig. 2 A cancer-CAF spheroid in the three-dimensional (3D) cell-sheet model shows more invasive characteristics. (A) A cartoon showing a 3D cell-sheet model mimicking epithelial cancer *in vivo*. (B) The growth and incsion of green fluorescent protein (GFP)-tagged cancer spheroid with or without CAFs (C only) in the 3D cell-sheet model. (C) Invasion of cancer spheroid with or without CAFs into the fibrin matrix in the 3D cell sheet. Bars in spheroid images indicate 100 μm. (D-F) Changes of viability, size, and growth area of the spheroid with or without CAFs grown in the 3D cell-sheet model and then exposed to 10 μM sorafenib or 20 μM cisplatin. The cancer area included the spheroid plus the invasion region into the fibrin matrix. The spheroid size and cancer area were compared with those on day 0. The error bars represent the standard deviation from three replicates. * P<0.05, ** P<0.01 relative to the control or C only.

3.3. Visualization of cancer cell viability, apoptosis, and hypoxia in the 3D cell-sheet model

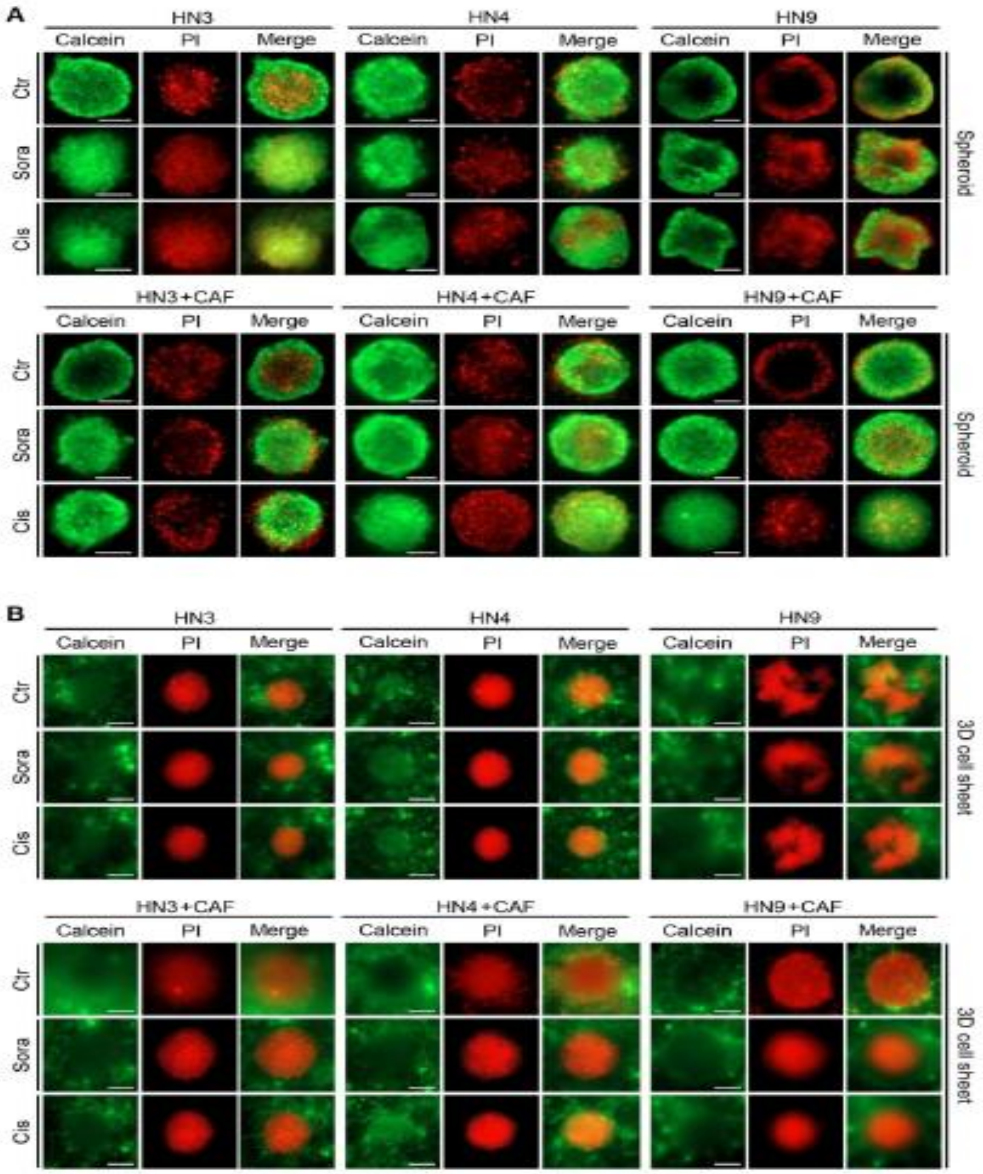

Figure 3. Expansion of viable cancer cells is increased in the three-dimensional (3D) cell-sheet model. Calcein-AM (green) and propidium iodide (PI, red) allow observation of viable and dead cells in the cancer spheroid (A) and 3D cell-sheet model (B) with or without CAFs. The spheroid and 3D cell sheet were exposed to vehicle control (ctr), 10 μM sorafenib, or 20 μM cisplatin for 72 h. The area of viable cells was larger in the 3D cell sheet than in the cancer spheroid because of a more peripheral spread of cancer cells in the 3D cell-sheet model. Bars indicate 100 μm.

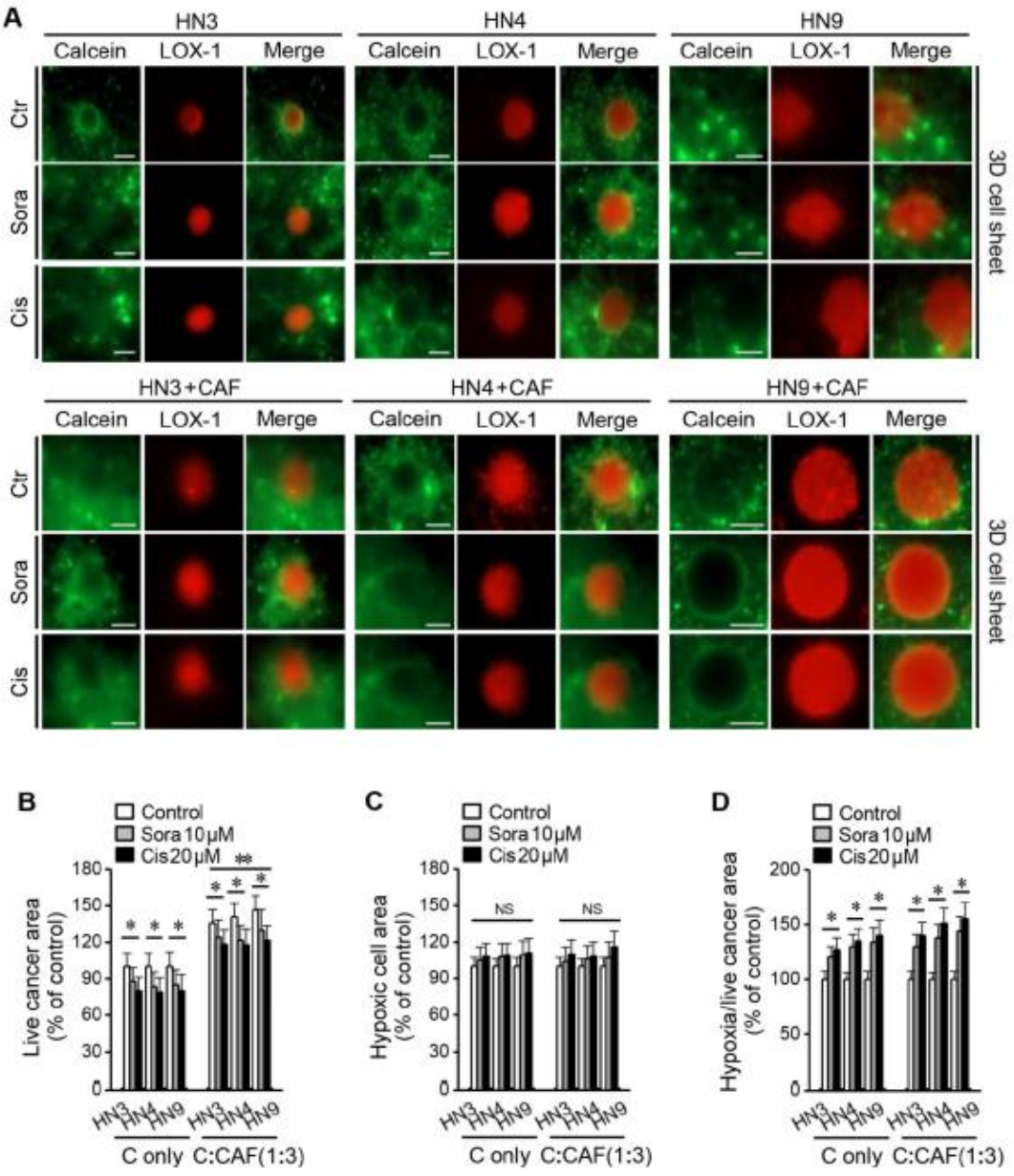

Figure 4. Hypoxia observed in the 3D cell-sheet model. (A) Hypoxic cells were detected with LOX-1 staining (red) and live cells with calcein-AM (green). (B) Areas of live and hypoxic cells were measured in the 3D cell sheet with or without CAFs (C only) at 72 h after exposure to vehicle control, 10 μM sorafenib, or 20 μM cisplatin. The areas of live cells in the cancer-CAFs or treatment groups were compared to the control of C only and the hypoxic cell areas were relative to the control of C only or the C:CAF group. Bars indicate 100 μm. The error bars represent the standard deviation from three replicates. *P < 0.05 relative to the control or the C only.

Figure3 shows viable and dead cells in cancer spheroids and 3D cell sheets after calcein-AM and PI staining, respectively. Viable cancer cells appeared to be more expanded than the cancer spheroid in the 3D cell-sheet model. In addition, hypoxic area was observed after LOX-1 staining in the center of cancer spheroid that was embedded into the 3D cell sheet (**Figure 4A**). The live cancer area was observed to be significantly larger in the 3D cell sheet with CAFs because the cancer spheroid with CAFs showed enhanced growth from its periphery into the surrounding region ($P<0.01$) (**Figure 4B**). Although the live cancer area significantly decreased in both cell sheets with and without CAFs, it was larger in those with CAFs, regardless of sorafenib or cisplatin treatment ($P<0.05$) (**Figure 4C**); however, the proportion of the hypoxic area to the live cancer area after drug treatment was significantly enlarged in cell sheets with and without CAFs because the treatment significantly decreased the live growing area ($P<0.05$) (**Figure 4D**).

3.4. Molecular expression levels in spheroids and cell sheets with or without CAFs

The relative mRNA levels of TGB1, CDH2, and VIM were significantly higher in cancers grown in the 3D cell sheet than in 2D monolayers or cancer spheroids, for all three HNC cell lines ($P<0.05$) (**Figure 5A-C**). The mRNA levels were also higher in cancer cells grown in the 3D cell sheet with CAFs than in those grown in sheet without CAFs ($P<0.05$). The protein levels of TGF-β1, N-cadherin, and vimentin were also much higher in cancer cells grown or cancer spheroids ($P<0.05$) (**Figure 5D**). The protein levels also appeared to be higher in cancer cells grown in the 3D cell-sheet model than in the cancer spheroid alone, and in 3D cell sheets with CAFs than in those without CAFs.

3.5. Comparing of stability between 3D cell-sheet model and 2D model/non-matrix model.

The stability of the 2D model and the 3D model was compared. In the 2D model, survival rates tended to decrease gradually (**Figure. 6A and 6C**) Also, we saw that the size of the cancer tissue decreased significantly after five days (**Figure 6B**). However, for the 3D cell-sheet model, survival rates remained similar to the initial level, and the area size of the cancer tissue did not decrease with non-matrix model (**Figure 7A, 7C, and 7D**).

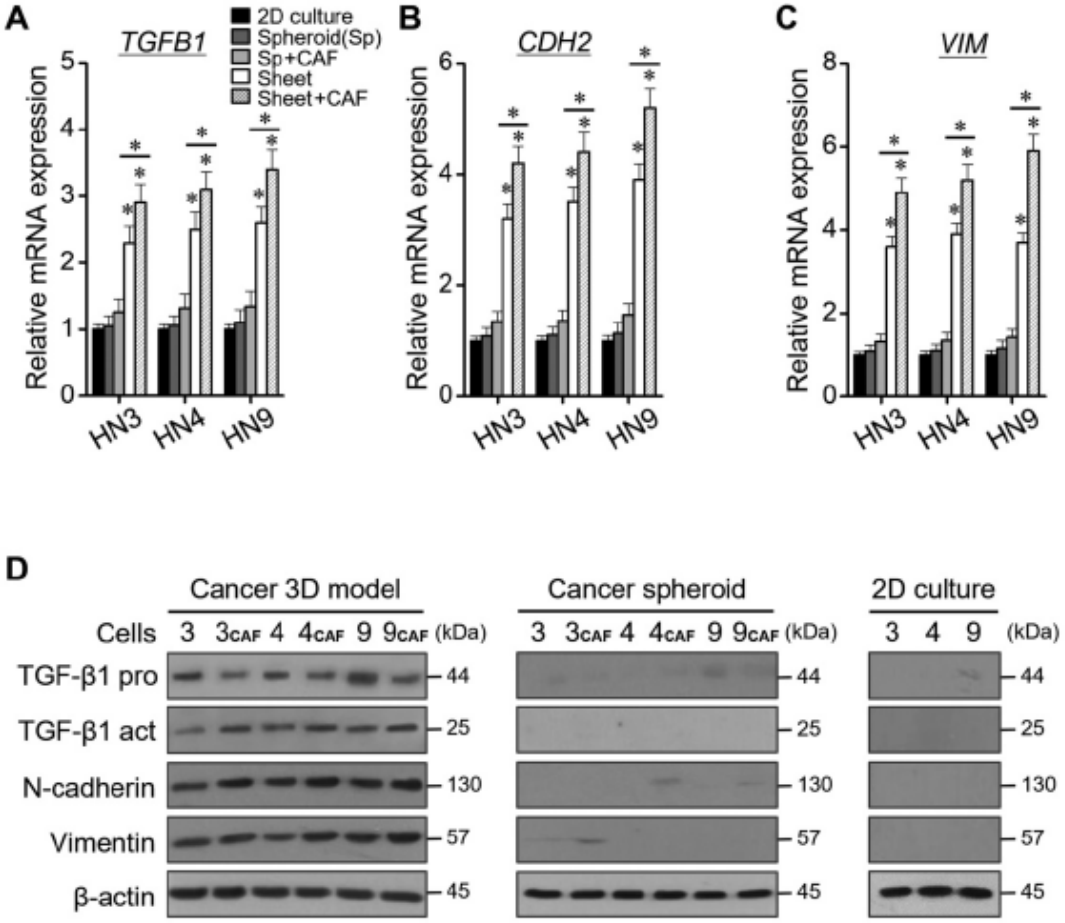

Figure 5. Levels of relative mRNA and protein expression according to 2D monolayer culture, spheroid, 3D cell sheet, and CAF incorporation. (A-C) Quantification of TGB1, CDH2, and VIM mRNAs. The error bars represent the standard deviation from three replicates. *P < 0.05 relative to the control or between cell sheet groups. (D) Western blotting of TGF-β1 (pro- and active forms), N-cadherin, and vimentin protein expression. β-actin was the loading control.

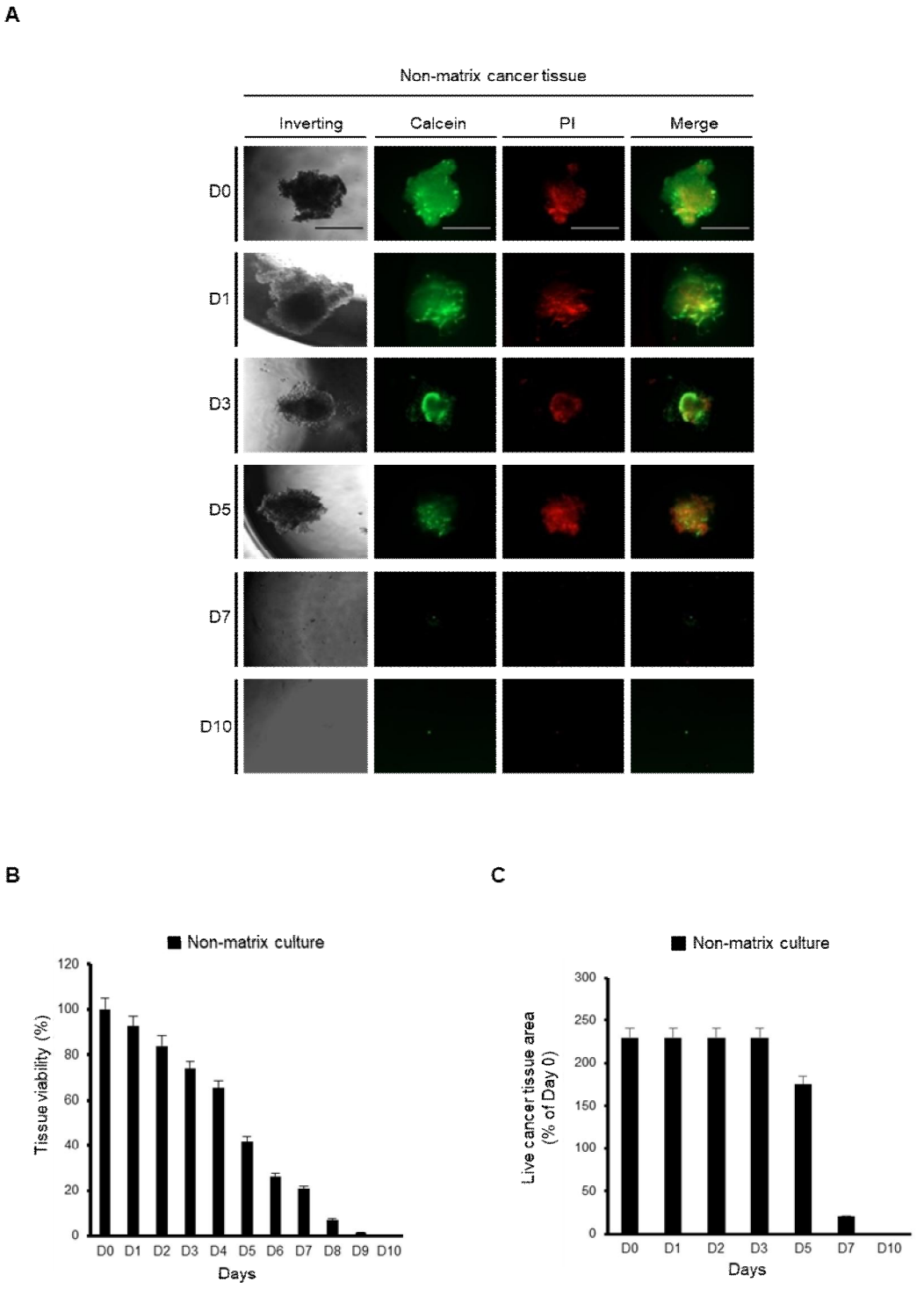

Figure 6. Estimating of stability in non-matrix tissue model. (A) The change of non-matrix tissue model by immunofluorescense for 10 days. (B) Tissue viability of non-matrix tissue model by CCK assay. (C) The areas of live tissue was measured in non-matrix tissue model. The error bars represent the standard deviation from three replicates. The error bars represent the standard deviation from three replicates. Bars indicate 200 μm.

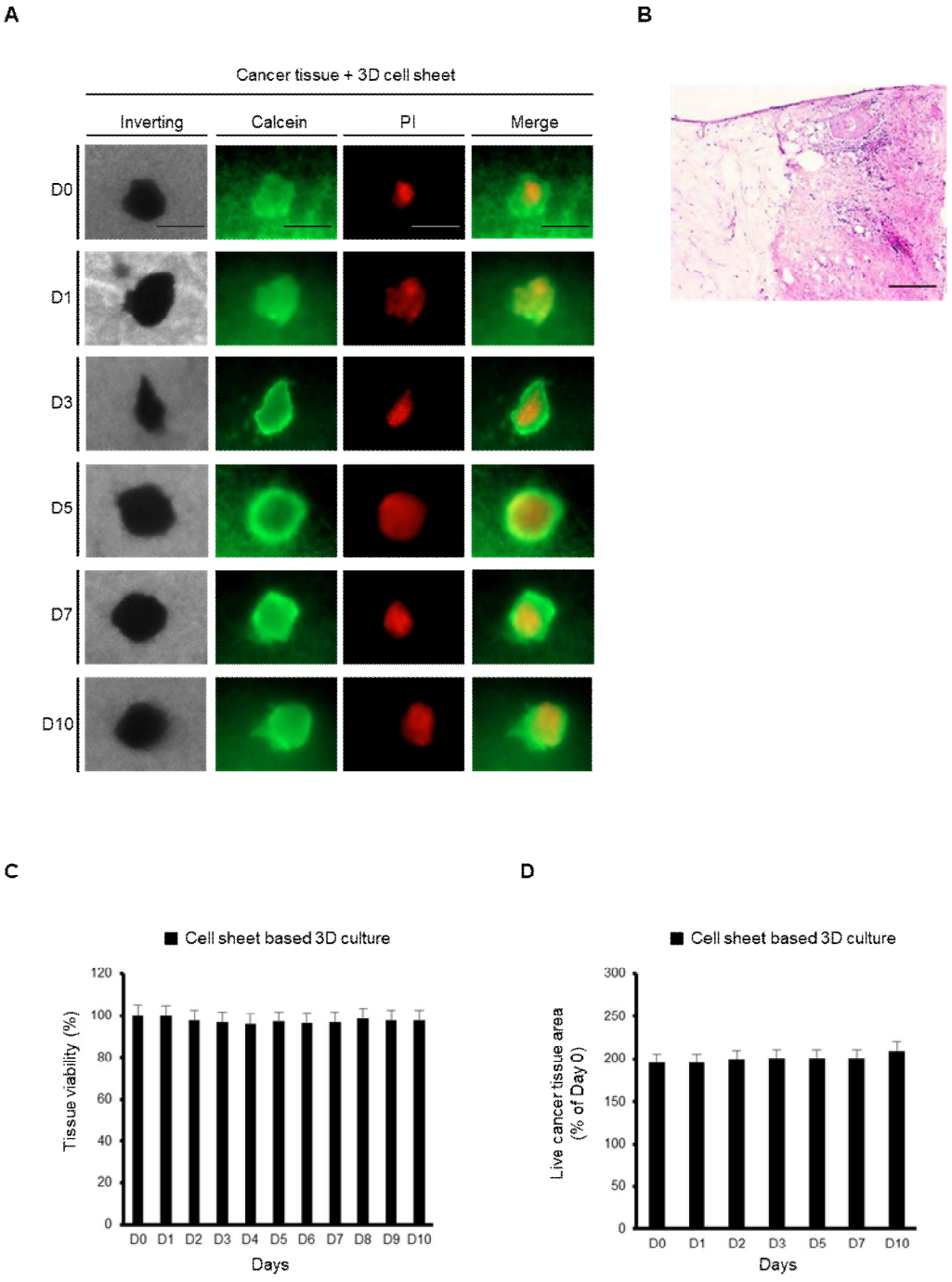

Figure 7. Assessing stability of 3D cell-sheet model. (A) The estimating stability of 3D cell-sheet model by immunofluorescence for 10 day. (B) The representative histological image using H&E staining in the 3D cell-sheet model (C) Tissue viability of 3D cell-sheet model by CCK assay. (D) The areas of live tissue were measured in 3D cell-sheet model. The error bars represent the standard deviation from three replicates. Bars indicate 200 μm (A), 100 μm (B).

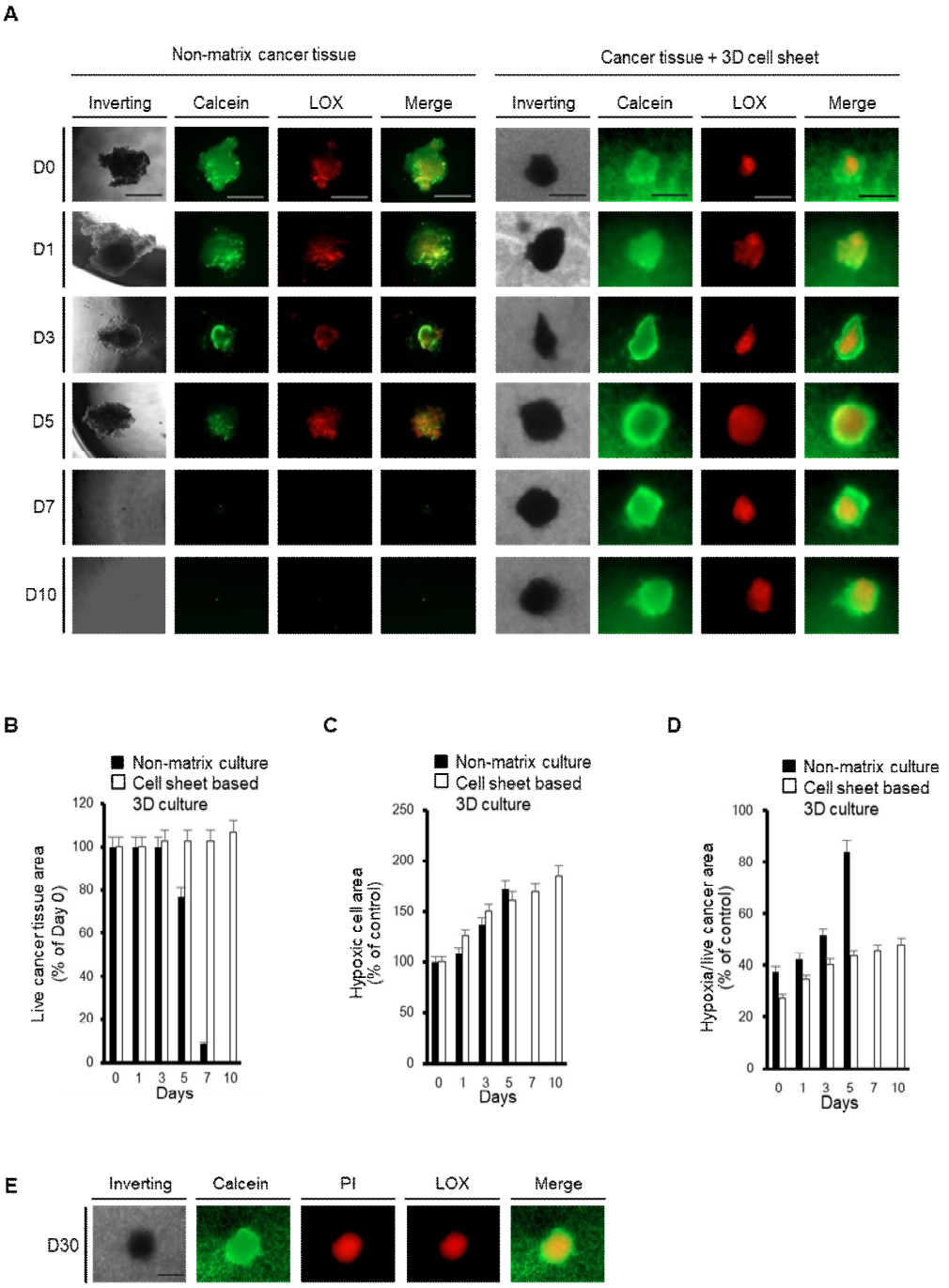

Figure 8. Hypoxia observed in non-matrix model and 3D cell-sheet model. (A) Hypoxic region was detected with LOX-1 staining (red) and live region with calcein-AM (green) in non-matrix model and 3D cell-sheet model. (B and C) Areas of live tissue and hypoxic tissue were measured in both models. (D) The ratio of Hypoxia to live cancer tissue area. (E) The representative image of live tissue in 3D -cell sheet model at 30 days. The error bars represent the standard deviation from three replicates. Bars indicate 200 μm.

3.6. Visualization and comparison of cancer tissue hypoxia in the 3D cell-sheet model

According to observations in the live and hypoxia region, by the 10 days, live area showed a slight increase in the 3D cell-sheet model, while the non-matrix model gradually declined from day 5 (**Figure 8A-B**). Although the hypoxia portion of the non-matrix model showed an increase from day 5, the hypoxia portion could not be observed after seven days due to tissue disintegration by an increase in necrosis in the tissue (**Figure 8C-D**). However, the 3D cell-sheet model allowed us to observe the hypoxia section at 30 days and confirm that the tissue form was maintained (**Figure 8E**).

3.7. Observing the effect of anti-cancer drug in tumor along concentration

The viability of cancer tissues following treatment of Cisplatin and docetaxel in 3D cell-sheet models showed that viability decreased to less than 10% in five days at 20, 50 uM (**Figure 9 and 10**)

3.8. The change of tumor appearance by anti-cancer drug

In the tissue transfected with GFP, by day 5, the cisplatin treatment group saw a 50% decrease in live tissue area compared to control, and the docetaxel group also had a similar tendency (**Figure 11A and 11B**). Dead tissue area showed an increase of about 4 times in cisplatin and docetaxel than that of control (**Figure 11C**). The ratio of dead parts of live Tissue area showed a ninefold increase compared to control (**Figure 11D**).

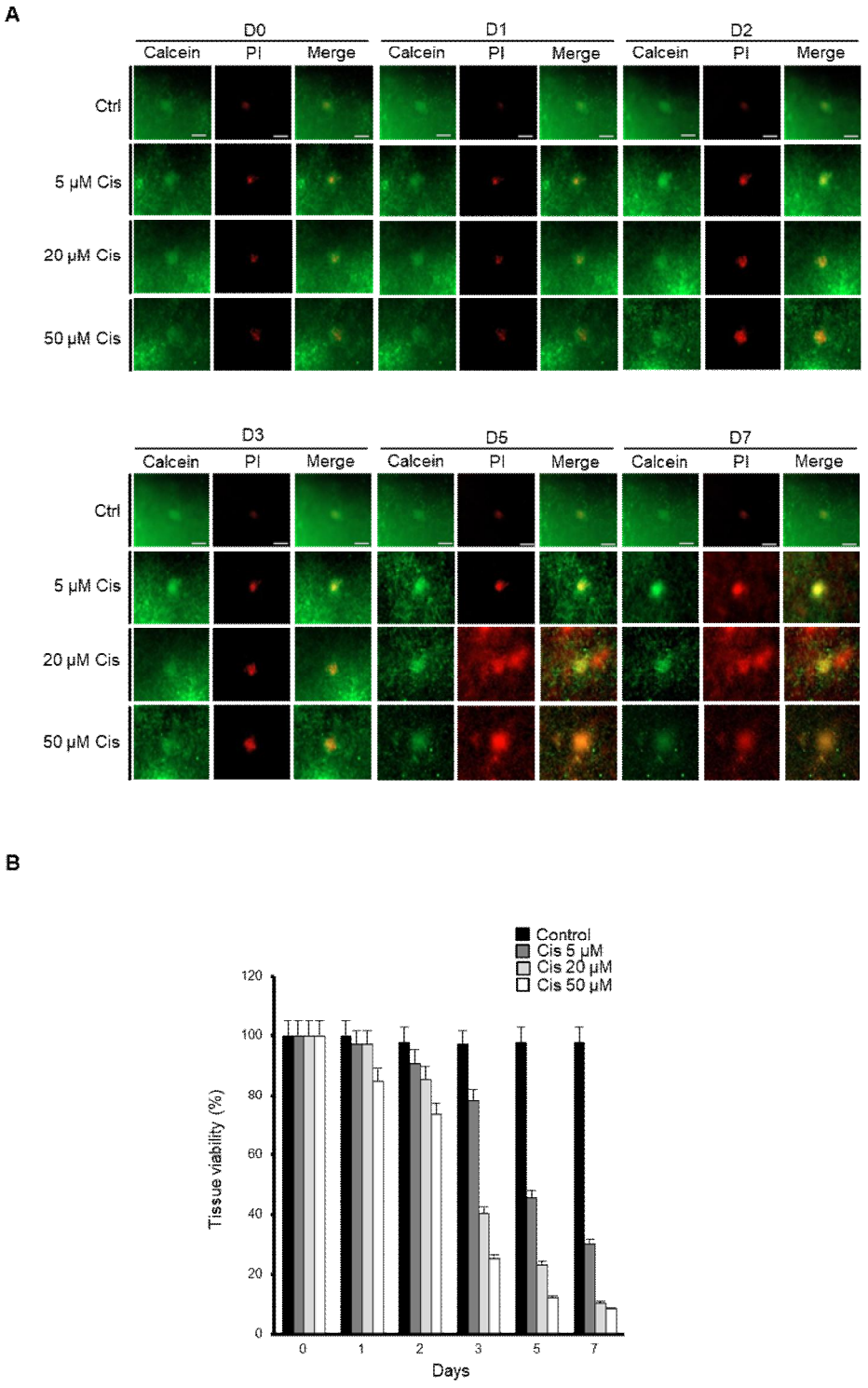

Figure 9. Dose dependent response of 3D cell-sheet model using cisplatin. (A) The representative image of immunofluorescence (B) Viability of 3D cell-sheet model by CCK assay. The error bars represent the standard deviation from three replicates. Bars indicate 200 μm.

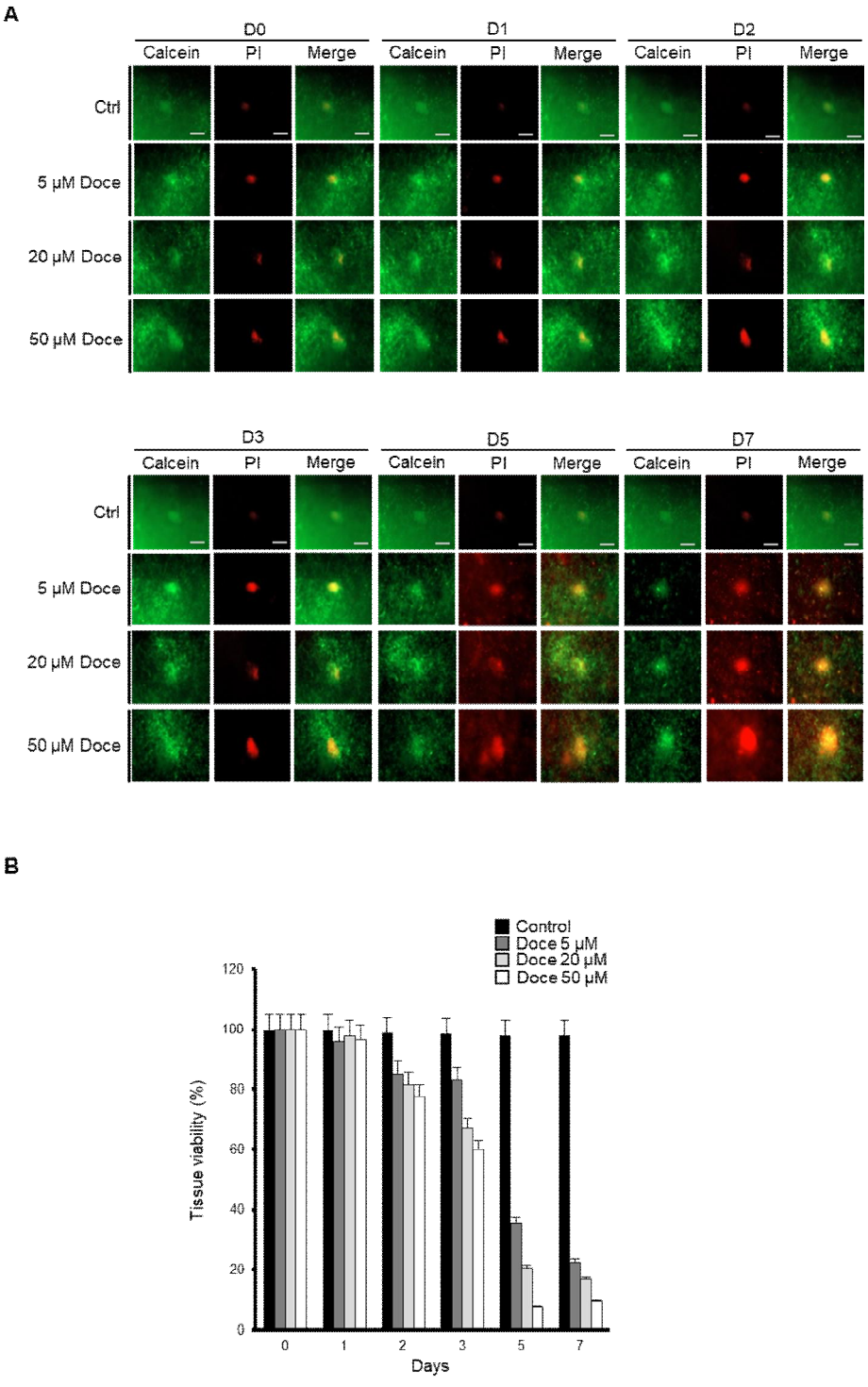

Figure 10. Dose dependent response of 3D cell-sheet model using docetaxel. (A) The representative image of immunofluorescence (B) Viability of 3D cell-sheet model by CCK assay. The error bars represent the standard deviation from three replicates. Bars indicate 200 μm.

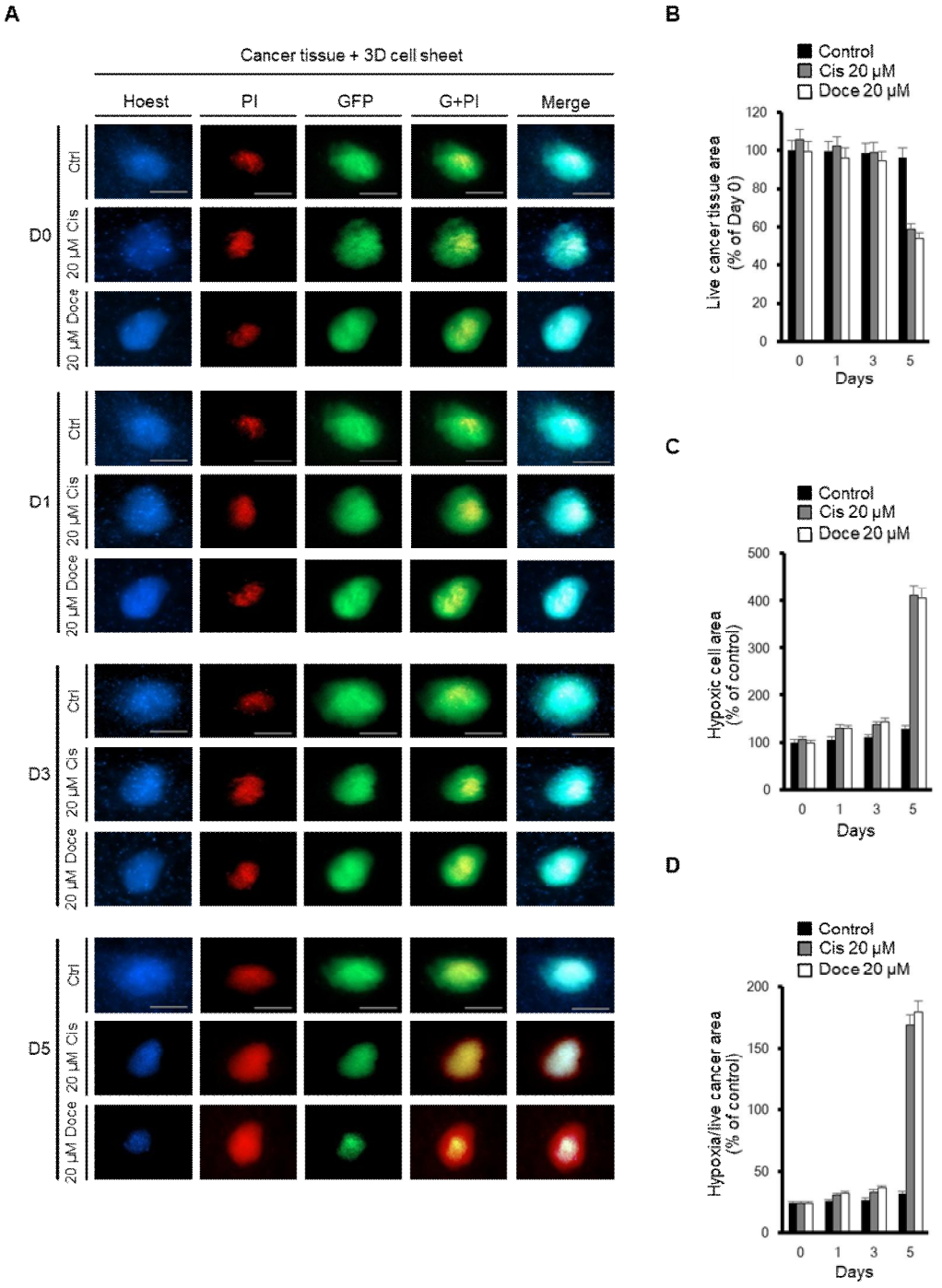

Figure 11. The morphologic change of GFP transfected cancer tissue in 3D cell-sheet model. (A) The representative image of drug responsive tissue using immunofluorescence for 5 days. (B and C) The area of live tissue and dead tissue were measured in the 3D cell-sheet model. (D) The ratio of dead to live cancer tissue area. The error bars represent the standard deviation from three replicates. Bars indicate 200 μm.

4. Discussion

The present study showed the usefulness of a 3D cell-sheet model that was tested for cancer growth, invasion, and anticancer drug screening. We developed a new 3D cell-sheet model that included a cancer spheroid interposed between oral keratinocytes and plasma fibrin with oral fibroblasts. Cancer-CAFs in the new 3D cell-sheet model showed enhanced invasive characteristics and resistance to chemotherapeutic agents. The expansion of viable cancer cells into the adjacent extracellular matrix with oral fibroblasts was greater in the 3D cell-sheet model than in a 2D model or cancer spheroid. Hypoxia was observed in the cancer spheroid grown in the 3D cell-sheet model. The mRNA and protein levels of proliferation and invasion markers, TGF-β1, N-cadherin, and vimentin, were higher in cancer cells grown in the 3D cell sheet; therefore, our study showed the potential applicability of our new model to reliable anticancer drug testing. Our newly developed 3D cell-sheet model for anticancer drug testing involved embedding a cancer spheroid into an oral mucosal cell sheet. We previously developed an in vitro engineered autologous mucosal cell sheet consisting of oral keratinocytes and plasma fibrin containing oral mucosal fibroblasts [17-19]. The mucosal cell sheet promoted wound healing in the oral cavity and skin, with minimal scar formation [18, 19]. Furthermore, we developed a 3D cell-sheet model with cancer alone or cancer-CAFs interposed between keratinocyte and fibrin–fibroblast layers. Epithelial cancers arising in the upper aerodigestive tract commonly initiate in the basal stem-cell layer of the epithelium, grow over the basement membrane, and invade into local surrounding tissues [11]. Our newly developed model provides structural and histological similarities withepithelial cancers, showing the close relationshipamong cancer cells, CAFs, and the extracellular matrix and fibroblasts. A biomimetic model with fibrin gel is known to be an applicable 3D culture system by which to screen anticancer drug efficacy by observing changes in proliferation, invasion, and migration of cancer spheroid cells [20, 21]. Our model involved fibrin from blood plasma that contained oral fibroblasts, which facilitate the induction of collagen and vessel formation in wounds [22, 23], and might provide an appropriate mimic of the tumour microenvironment in vivo. The microenvironment including keratinocytes might also direct cancer spheroid cells into epithelial-mesenchymal transition (EMT) [24]. Our study showed that spheroid and CAFs promoted cancer cell resistance to cisplatin and sorafenib. For anticancer drug screening, cancer cells are commonly cultured in a 2D monolayer in a flat-bottomed plate. A multicellular spheroid model has been shown to more reliably predict the clinical responses of cancers to agents [25, 26]. A previous study showed that

proliferation rates were more divergent in HNC cells grown in a 3D model than those in a 2D model, which might contribute to the observed differential response rates to increasing doses of cisplatin and irradiation [25]. Immunohistochemical analyses of proliferation and angiogenesis protein markers might better reflect the characteristics of cancers grown in 3D spheroid culture than in those grown in 2D culture [25]. A recent study also showed that HNC cells in 2D culture led to death by plasma-activated medium and H_2O_2; however, 3D tumour spheroids were rapidly regrown to be resistant to that treatment [26]. The different results in 2D and 3D culture systems might be explained by the fact that the 3D tumour microenvironment modulates the anticancer drug response [27]. In addition, CAFs are known to contribute to acquired chemotherapeutic resistance in cancer cells through the interaction between cancer cells and stroma [28, 29]. CAFs have been suggested to protect cancer cells from cetuximab treatment by inducing MMP-1 [30]. An escape from cancer therapy can be mediated by the adhesion of cancer cells to the extracellular matrix proteins collagen, laminin, and fibronectin [31]. CAFs also increase hyaluronan production, which increases resistance in drug-sensitive cancer cells [32]. CAFs function in a manner similar to that of myofibroblasts that secrete interleukin-6 (IL-6), which plays an important role in tumour proliferation, migration, and angiogenesis [33]. An increase in IL-6 promotes cancer-cell metastasis by inducing EMT [34]. Our study supported the previous findings that CAF incorporation into a cancer spheroid enhances resistance to chemotherapeutic agents. Furthermore, our new model allows examining the growth and invasion of cancer cells by mimicking the in vivo tumour microenvironment better than either the 2D monolayer model or the 3D cancer spheroid alone. The cancer-CAF spheroid in our new 3D cell-sheet model showed enhanced invasive characteristics. The increased local invasion of cancer spheroid cells might also be reflected by the increase in cell proliferation levels and EMT markers. Our data from the new 3D model support the previous suggestion that the examination of mutual interplay between the tumour and its microenvironment is crucial in cancer research [35]. A synergistic interaction between the tumour and its microenvironment facilitates tumour growth and dissemination, as first suggested in Paget's "seed and soil" hypothesis [36]. The fibrin matrix and CAFs promote EMT of cancer spheroid cells by losing epithelial properties and gaining invasive mesenchymal properties [35, 36]. Furthermore, our model provides improved therapeutic evaluation of anticancer drugs. A previous report showed that the efficacy of drugs is better examined in a multicellular tumour spheroid that is cultured in collagen matrix gel [37]. 3D biomimetic model can also examine the resistance of epithelial cancer cells to various drugs by exploring cell–

matrix interactions [38]. In addition, the 3D model allow for stable long-term culture, reportedly for up to 28 days, and reflect the pathophysiological events in cancer patients in terms of the evaluation of anticancer chemosensitivity better than 2D monolayers [39]. Hypoxia was also observed in the cancer spheroids in our 3D model system. The increase in the hypoxic area relative to the total cancer area in our study might be associated with resistance to sorafenib or cisplatin. A previous study suggested that the extent and pattern of hypoxia within multicellular tumour spheroids that are cultured in a 3D collagen matrix help in evaluating tumour phenotypic function and anticancer drug screening [40]. Drug resistance can be mediated by functional interactions between hypoxia-inducible factors and cell-death pathways in hypoxic tumour spheroid cells and the surrounding matrix [40, 41]. Our 3D model system might also provide information to help improve sensitivity to anticancer drugs on the basis of hypoxia in tumour spheroids cultured in the 3D cell-sheet model. Drug penetration into and metabolism by cancer cells might be questionable in the 3D culture system; however, this issue can be resolved by introducing a microfluidic system into the 3D culture model [42]. Microfluidic 3D models include endothelial sprouts and neovessels with pro-angiogenic factors, allowing vessel formation and drug delivery to the tumour spheroids [43]. A co-culture with endothelial cells in the tumour spheroid or matrix allows for new vessel formation, the initiation of EMT, and the mobilization of tumour cells [44]. The 3D cell-sheet model containing endothelial cells might better replicate the physiological landscape of tumour tissue in vivo; therefore, our new 3D model will be further developed to include endothelial progenitor cells within the fibrin matrix layer containing fibroblasts [45]. This would provide a tumour microenvironment that more comprehensively mimics the progression of human solid tumours than our current 3D model does and should be examined in further studies. In addition, in vitro models mimicking the observed side effects of and resistance to drugs might be very useful and should be examined in future studies.

The tissue explant culture model was already known, such as PDX, slice culture, and scaffold model. However, each model has constantly raised the issues like maintenance costs, heterogeneity, long-term culture and the form of tumor microenvironment. [46, 47] Our model was made as a model to overcome these limitations. As shown in the results, our model showed that even for 30 days tissue culture had a low viability reduction and the tissue form and characteristics were maintained. We think this could help us observe the long-term physiological shape of cancer. In addition, the live/dead assay using the calcin_AM and propidium iodide (PI) could be used to observe the live area along time. In the tissue response to

Cisplatin and docetaxel, we were able to compare their form, dead, and live without such procedures as fixation, and we were able to reduce the difference. The ease and stability of this observation is important as a pre-clinical test to apply to actual patients and we believe that it will help in the drug selection of chemotherapy in the future. However, our model has to cut the tissue to a small degree about ~400 μm. In doing so, it is difficult to select a certain size tissue fragments, and the number of cancer in the tissue might be also smaller than the overall metric tissue culture. To overcome these limitations, the GFP was introduced to the finely chopped tissue, as the alternative method by which we could choose the tissue that have the sufficient number of cancer and achieved some results. In addition, the introduction of GFP allowed us to check the extent of the live without the use of a separate calcin AM. However, the problem is that tissue have their fluorescence capabilities so, we have to find ways to minimize it. On top of that, it is difficult to tell whether the cells that are introduced by GFP are CAF or Cancer. Future research will need to overcome the aforementioned limitations and create a framework for studying the interactions with the surrounding tissues that have recently emerged in addition to the short-term drug-assessment areas.

5. Conclusion

The present study showed the potential of our newly developed 3D epithelial cancer model produced by in vitro cell-sheet engineering for comparing the results of chemotherapeutic drug screening among the 3D cell-sheet model, spheroid culture, and 2D cell culture. Cancer cells and CAFs showed more extensive growth and invasion into the adjacent fibrin matrix in our 3D cell-sheet model. Cancer-CAF spheroids grown in the 3D cell-sheet model were more resistant to several chemotherapeutic agents, and the model provided molecular evidence of increased levels of proliferation and EMT markers; therefore, our 3D cell-sheet model might be applicable to in vitro observation of epithelial cancer growth and invasion and to anticancer drug testing.

6. References

[1] Waseem Asghar et al. Engineering cancer microenvironments for in vitro 3-D tumor models. Materials Today. 2015; 18: 539-553.

[2] L.P. Ferreira, V.M. Gaspar, J.F. Mano. Design of spherically structured 3D in vitro tumor models –Advances and prospects. Acta Biomaterialia. 2018; 75: 11-34.

[3] Tatiana A. Karakasheva et al. IL-6 mediates cross-talk between tumor cells and activated fibroblasts in the tumor microenvironment. Cancer Res. 2018; 78(17):4597-4970.

[4] Michele De Palma, Daniela Biziato & Tatiana V. Petrova. Microenvironmental regulation of tumour angiogenesis. Nature review cancer. 2017; 17:457-474.

[5] Ferenc Sipos and Orsolya Galamb. Epithelial-to-mesenchymal and mesenchymal-to-epithelial transitions in the colon. World J Gastroenterol. 2012; 18(7): 601-608.

[6] Cukierman E, Pankov R, Stevens DR, Yamada KM. Taking cell-matrix adhesions to the third dimension. Science. 2001; 294: 1708-12.

[7] Xu X, Farach-Carson MC, Jia X. Three-dimensional in vitro tumor models for cancer research and drug evaluation. Biotechnol Adv. 2014;32:1256-68.

[8] Unger C, Kramer N, Walzl A, Scherzer M, Hengstschlager M, Dolznig H. Modeling human carcinomas: physiologically relevant 3D models to improve anti-cancer drug development. Adv Drug Deliv Rev. 2014;79-80:50-67.

[9] Costa EC, Moreira AF, de Melo-Diogo D, Gaspar VM, Carvalho MP, Correia IJ. 3D tumor spheroids: an overview on the tools and techniques used for their analysis. Biotechnol Adv. 2016;34:1427-41.

[10] Nath S, Devi GR. Three-dimensional culture systems in cancer research: Focus on tumor spheroid model. Pharmacol Ther. 2016;163:94-108.

[11] Tang XH, Scognamiglio T, Gudas LJ. Basal stem cells contribute to squamous cell carcinomas in the oral cavity. Carcinogenesis. 2013;34:1158-64.

[12] Lu TL, Huang YF, You LR, Chao NC, Su FY, Chang JL, et al. Conditionally ablated Pten in prostate basal cells promotes basal-to-luminal differentiation and causes invasive prostate cancer in mice. Am J Pathol. 2013;182:975-91.

[13] Murata T, Mizushima H, Chinen I, Moribe H, Yagi S, Hoffman RM, et al. HB-EGF and PDGF mediate reciprocal interactions of carcinoma cells with cancer-associated fibroblasts to support progression of uterine cervical cancers. Cancer Res. 2011;71:6633-42.

[14] Joyce JA, Pollard JW. Microenvironmental regulation of metastasis. Nat Rev Cancer. 2009;9:239-52.

[15] Psaila B, Lyden D. The metastatic niche: adapting the foreign soil. Nat Rev Cancer. 2009;9:285-93.
[16] Knobloch J, Ruther U. Shedding light on an old mystery: thalidomide suppresses survival pathways to induce limb defects. Cell Cycle. 2008;7:1121-7.
[17] Roh JL, Lee J, Jang H, Kim EH, Shin D. Use of oral mucosal cell sheets for accelerated oral surgical wound healing. Head Neck. 2018;40:394-401.
[18] Roh JL, Jang H, Lee J, Kim EH, Shin D. Promotion of oral surgical wound healing using autologous mucosal cell sheets. Oral Oncol. 2017;69:84-91.
[19] Roh JL, Lee J, Kim EH, Shin D. Plasticity of oral mucosal cell sheets for accelerated and scarless skin wound healing. Oral Oncol. 2017;75:81-8.
[20] Bayat N, Ebrahimi-Barough S, Norouzi-Javidan A, Saberi H, Tajerian R, Ardakan MMM, et al. Apoptotic effect of atorvastatin in glioblastoma spheroids tumor cultured in fibrin gel. Biomed Pharmacother. 2016;84:1959-66.
[21] Bayat N, Ebrahimi-Barough S, Norouzi-Javidan A, Saberi H, Ardakan MMM, Ai A, et al. Anti-inflammatory effects of Atorvastatin by suppressing TRAF3IP2 and IL-17RA in human glioblastoma spheroids cultured in a three-dimensional model: Possible relevance to glioblastoma treatment. Mol Neurobiol. 2018;55:2102-10.
[22] Sclafani AP, McCormick SA. Induction of dermal collagenesis, angiogenesis, and adipogenesis in human skin by injection of platelet-rich fibrin matrix. Arch Facial Plast Surg. 2012;14:132-6.
[23] Martinez-Santamaria L, Conti CJ, Llames S, Garcia E, Retamosa L, Holguin A, et al. The regenerative potential of fibroblasts in a new diabetes-induced delayed humanised wound healing model. Exp Dermatol. 2013;22:195-201.
[24] Chandrasekaran S, Giang UB, King MR, DeLouise LA. Microenvironment induced spheroid to sheeting transition of immortalized human keratinocytes (HaCaT) cultured in microbubbles formed in polydimethylsiloxane. Biomaterials. 2011;32:7159-68.
[25] Kadletz L, Heiduschka G, Domayer J, Schmid R, Enzenhofer E, Thurnher D. Evaluation of spheroid head and neck squamous cell carcinoma cell models in comparison to monolayer cultures. Oncol Lett. 2015;10:1281-6.
[26] Nofel M, Chauvin J, Vicendo P, Judee F. Effects of Plasma Activated medium on head and neck FaDu cancerous cells: comparison of 3D and 2D response. Anticancer Agents Med Chem. 2017.
[27] Ekert JE, Johnson K, Strake B, Pardinas J, Jarantow S, Perkinson R, et al. Three-dimensional lung tumor microenvironment modulates therapeutic compound responsiveness in vitro--implication for drug development. PLoS One. 2014;9:e92248.
[28] Li XY, Hu SQ, Xiao L. The cancer-associated fibroblasts and drug resistance.

Eur Rev Med Pharmacol Sci. 2015;19:2112-9.
[29] Meads MB, Gatenby RA, Dalton WS. Environment-mediated drug resistance: a major contributor to minimal residual disease. Nat Rev Cancer. 2009;9:665-74.
[30] Fiaschi T, Giannoni E, Taddei ML, Cirri P, Marini A, Pintus G, et al. Carbonic anhydrase IX from cancer-associated fibroblasts drives epithelial-mesenchymal transition in prostate carcinoma cells. Cell Cycle. 2013;12:1791-801.
[31] Paraiso KH, Smalley KS. Fibroblast-mediated drug resistance in cancer. Biochem Pharmacol. 2013;85:1033-41.
[32] Misra S, Ghatak S, Zoltan-Jones A, Toole BP. Regulation of multidrug resistance in cancer cells by hyaluronan. J Biol Chem. 2003;278:25285-8.
[33] Nagasaki T, Hara M, Nakanishi H, Takahashi H, Sato M, Takeyama H. Interleukin-6 released by colon cancer-associated fibroblasts is critical for tumour angiogenesis: anti-interleukin-6 receptor antibody suppressed angiogenesis and inhibited tumour-stroma interaction. Br J Cancer. 2014;110:469-78.
[34] Yadav A, Kumar B, Datta J, Teknos TN, Kumar P. IL-6 promotes head and neck tumor metastasis by inducing epithelial-mesenchymal transition via the JAK-STAT3-SNAIL signaling pathway. Mol Cancer Res. 2011;9:1658-67.
[35] Catalano V, Turdo A, Di Franco S, Dieli F, Todaro M, Stassi G. Tumor and its microenvironment: a synergistic interplay. Semin Cancer Biol. 2013;23:522-32.
[36] Paget S. The distribution of secondary growths in cancer of the breast. 1889. Cancer Metastasis Rev. 1989;8:98-101.
[37] Moustakas A, Heldin CH. Signaling networks guiding epithelial-mesenchymal transitions during embryogenesis and cancer progression. Cancer Sci. 2007;98:1512-20.
[38] Le VM, Lang MD, Shi WB, Liu JW. A collagen-based multicellular tumor spheroid model for evaluation of the efficiency of nanoparticle drug delivery. Artif Cells Nanomed Biotechnol. 2016;44:540-4.
[39] Loessner D, Stok KS, Lutolf MP, Hutmacher DW, Clements JA, Rizzi SC. Bioengineered 3D platform to explore cell-ECM interactions and drug resistance of epithelial ovarian cancer cells. Biomaterials. 2010;31:8494-506.
[40] Ma J, Zhang X, Liu Y, Yu H, Liu L, Shi Y, et al. Patterning hypoxic multicellular spheroids in a 3D matrix - a promising method for anti-tumor drug screening. Biotechnol J. 2016;11:127-34.
[41] Rohwer N, Cramer T. Hypoxia-mediated drug resistance: novel insights on the functional interaction of HIFs and cell death pathways. Drug Resist Updat. 2011;14:191-201.
[42] LaBonia GJ, Lockwood SY, Heller AA, Spence DM, Hummon AB. Drug penetration and metabolism in 3D cell cultures treated in a 3D printed fluidic device:

assessment of irinotecan via MALDI imaging mass spectrometry. Proteomics. 2016;16:1814-21.
[43] Sung KE, Beebe DJ. Microfluidic 3D models of cancer. Adv Drug Deliv Rev. 2014;79-80:68-78.
[44] Ehsan SM, Welch-Reardon KM, Waterman ML, Hughes CC, George SC. A three-dimensional in vitro model of tumor cell intravasation. Integr Biol (Camb). 2014;6:603-10.
[45] Lee J, Kim EH, Shin D, Roh JL. Accelerated oral wound healing using a pre-vascularized mucosal cell sheet. Sci Rep. 2017;7:10667.
[46] M M Gerlach et al.Slice cultures from head and neck squamous cell carcinoma: a novel test system for drug susceptibility and mechanisms of resistance. BJC. 2014;110, 479-488.
[47] Carmela Ricciardelli et al. Novel ex vivo ovarian cancer tissue explant assay for prediction of chemosensitivity and response to novel therapeutics. Cancer letter 2018 ;421 51-58,

7. Supplementary figure

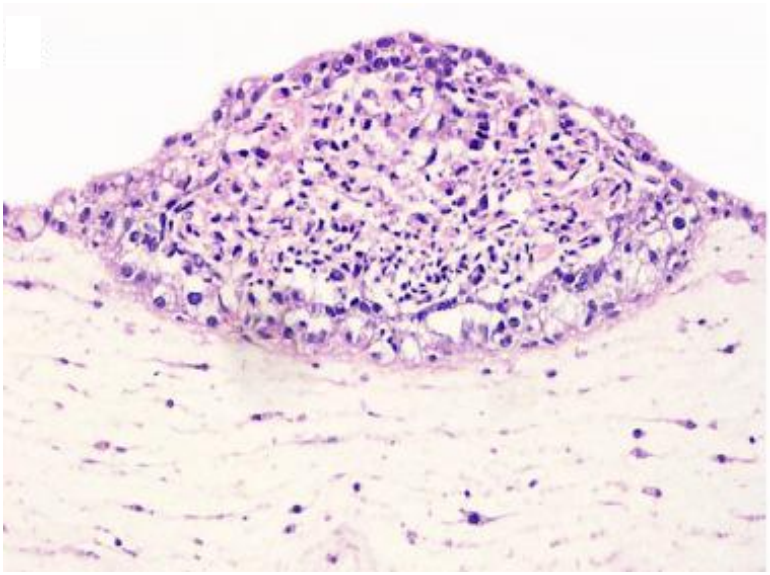

Figure S1. Histological examinations of spheroids and 3D cell-sheet model. Hisotology of th 3D cell-sheet model using Hematoxylin and eosin staining at day 0. Original maginifiction, 40x.

Abstract (in Korean)

세포시트 기반 생체외 암 모델의 개발

이재왕
의학과
울산대학교 대학원

암은 인간의 주요 죽음의 원인 중 하나이다. 암에 대한 연구는 20세기를 넘어 21세기인 현재까지 많이 진행되었지만 아직 암에 대하여 완전히 이해하지 못 하고 있다. 이러한 상황에서 개발된 2차원 모델은 많은 암 연구에 있어서 표준적인 모델으로서 사용되고 있지만, 이러한 2차원 모델은 실제 암의 환경을 반영하지 못하는 단점이 있다. 이러한 단점으로 인해 2차원 모델로 부터의 결과를 토대로 환자에게 적용하기엔 무리가 따르고 이를 극복하기 위해 실제 환경과 유사한 3D 모델들이 개발되고 있다. 하지만, 이러한 3차원 모델 또한 단지 암 세포를 가지고 spheroid라는 형태를 만들어 연구하는 방식이거나 다른 세포를 섞어 spheroid를 만들어 연구하는 형태를 띄고 있을 뿐, 실제 체내에서 존재하는 ECM 부분은 전혀 고려되고 있지 않은 상황이었다. 최근에 들어서야 이러한 부분들이 고려된 모델들이 개발되고 있고, 우리 또한 세포시트라는 자체 기술을 가지고 이러한 기류에 편승하여 세포시트 기반의 3차원 모델을 개발 하였다. 세포시트는 체내의 조직을 흉내 낸 인공조직으로 수술 후 발생하는 결손 부위, 화상, 당뇨환자의 아물지 않는 상처의 회복을 돕기 위해 개발 되었다. 세포시트를 spheroid와 결합하여 실제 암 환경과 유사한 환경을 인공적으로 만들 수 있다고 생각하여 연구를 진행 하였다. 우리의 연구 결과에서, 2차원 또는 단순 spheroid culture에서와는 다르게 세포시트의 ECM의 존재는 cancer에 항암제에 대한 저항성을 더 높여주는 모습을 보여 주었다. 또한, GFP가 transfection된 cancer cell로 만든 세포시트 결합 모델에서, 전자의 기존 모델들과는 다르게 세포시트 모델은 invasion과 주변으로의 퍼져나가는 모습을 확인 할 수 있었다. 또한, 기존의 3차원 모델들에서 관찰 할 수 있는 암의 주요 특징 중 하나인 내부의 hypoxia 지역을 관찰 할 수 있었다. EMT 관련 대표 분자인 vimentin, TGF-β1, N-cadherin을 RT-qPCR과 western blot을 통해 분석한 결과 vimentin과 N-cadherin, active TGF-β1은 증가하였고, N-cadherin은 감소하는 결과를 보여 나타내었다. 더 나아가 환자로부터 얻은 암 조직을 이용하여 만든 3차원 모델에서 기존 2차원 조직 모델에서 확립할 수 없었던 안정성을 30일 까지 확보 할 수 있었다. 또한 조직으로 GFP 도입을 통해 살아있는 부분을 형광현미경으로 실시간으로 확인 할 수 있었다. 이러한 점 5일간의 항암제 처리 반응에서 시간에 따른 암 조직에 대한 영향을 확인 할 수 있었다. 이것은 각 환자에 맞는 항암제 선정에 도움이 될 것으로 예상한다.

주제어: Head and neck 암, 약물 시험, 세포시트, 생체외 3 차원 모델, 침투